TECHNICAL PAPER

A micro-control capture images technology for the finger vein recognition based on adaptive image segmentation

Chih-Cheng Chiu[1] · Tung-Kuan Liu[2] · Weu-Ting Lu[3] · Wen-Ping Chen[3,4] · Jyh-Horng Chou[2,4,5]

Abstract

The advantages of finger-vein recognition, compared to other biometric recognition technology commonly enlisted in identification needs such as ATM and door security, are uniqueness and living recognition, and so it has recently become one of major topics in biometric investigation. Through the irradiation of near-infrared rays, the finger-vein images are generated by blood vessels, and the texture of the image is created by the level of transparency between skeleton joints of the finger. Feature extraction of most finger-vein images employs global characteristics instead of local characteristics. This paper presents a local features method for dealing with the four segmentation of finger-vein images according to the physiological characteristics of finger. The four segmentation will be separated by a dynamic boundary line determined by the global vertical statistical quantity of the finger-vein image. Afterwards, each segmentation will be added with weighted values to enhance the fidelity of recognition. This study employs a total of 3816 finger-vein images generated by 106 adults in age of 20–60 years. The forefinger, middle finger, and little finger of each adult will be sampled for six images. Finally, the average recognition proposed by this study reaches 97%. The significant accuracy and contribution of this study is illustrated when compared to methods of global feature extraction (74.55%) and fixed-four regional segmentation feature extraction (86.48%).

1 Introduction

Technological developments bring not only convenience, but also personal security issues (Li et al. 2017; Ohtake et al. 2015; Anjomshoa et al. 2017), requiring the successive invention of many identification methods. For example, radio frequency identification (RFID) has been applied into the management of warehousing, manufacturing, pharmaceuticals, and logistics (Jabbar et al. 2008). However, this recognition technology does not meet the growing need for identity protection from counterfeiting. Thus, biometric recognition technology, utilizing the individual characteristics of the human body, surged into the main stream of research (Ratha et al. 2015; Hong and Jain 1998). These technologies have been widely used for identification purposes to prevent unauthorized persons from accessing many platforms: personal mobile phones, ATM system, personal computers, workstations, computer network systems and so on.

Biometric recognition technology samples partial biological characteristics and converts the information into codes saved in the database for identity verification. These technologies are divided into two categories: physical and behavioral characteristics. Physical characteristics include facial features: retina, iris, palm shapes, fingerprints, veins, DNA, skeleton segments, and so on. Behavioral characteristics include signature, voiceprint, and other features. These biometric recognition technologies have their own advantages and drawbacks. For instance, iris recognition is highly specific due to the unique biological characteristics

✉ Wen-Ping Chen
 wpc@kuas.edu.tw

1 Ph.D. Program in Engineering Science and Technology, College of Engineering, National Kaohsiung First University of Science and Technology, Kaohsiung, Taiwan

2 Department of Mechanical and Automation Engineering, National Kaohsiung First University of Science and Technology, Kaohsiung, Taiwan

3 Graduate Institute of Clinical Medicine, Kaohsiung Medical University, Kaohsiung, Taiwan

4 Department of Electrical Engineering, National Kaohsiung University of Applied Sciences, Kaohsiung, Taiwan

5 Department of Healthcare Administration and Medical Informatics, Kaohsiung Medical University, Kaohsiung, Taiwan

of the eye (Ohtake et al. 2015). However, the cost of camera lens for gathering iris images is expensive. Meanwhile, the iris-recognition process has difficulty in extracting the features of people with darker irises without enough light source. Retina recognition also benefits from the unique biological characteristics of the eye (Jabbar et al. 2008). The retina employs the shape of micro vasculature behind the eyeball to carry out search and judgment. The advantages include fixed biometric characteristics and indirect contact with the instrument. Additionally, the process is less susceptible to the effects of wear, aging, and disease. However, one critical disadvantage is that the retinal texture must be captured and exposed by a special wavelength of light, consequently this recognition technology cannot be applied to patients with retinopathy. In comparison, the face recognition process carries out identification by analyzing the relationship of the facial characteristics (Ratha et al. 2015; Xing et al. 2015; Chiranjeevi et al. 2015; Li et al. 2015). The acumen of identification shall be improved by Artificial Intelligence (AI), such as neural networks, because of low uniqueness of biological characteristics (Chiranjeevi et al. 2015). The cost of extracting images is cheaper than retinal recognition and iris recognition. However, even though the images can be extracted by inexpensive devices, expensive equipment is required to capture facial images with the clarity necessary for security identification. Meanwhile, the accuracy of identification will be affected by the light source and position between catch and camera lens of facial characteristics.

The finger recognition technology has been maturing for years (Kai and Jain 2015; Jain et al. 2017; Hong and Jain 1998). Fingerprint features included the invariance, uniqueness, regeneration, preservation, and traceability, the last method, 'traceability,' is the most accurate present method of identification for judicial and medical authorities. This technology is divided into two major methodologies. One is the similarity of different fingerprint images compared by statistics. The other compares the inherent features of the fingerprint image. 'Fingerprint features' refers to the distribution of the protruding lines of fingerprints. Each protruding line has a fracture named 'endpoint.' In addition to the endpoint, bifurcation points still play an important role in finger recognition. However, for patients with hand dermatitis these fingerprint images are not easy to capture. The 'Signature recognition' method of identification has a long history (Jayasekara et al. 2006; Chang et al. 2003). It is a well-known concept to write down signatures in various documents as a form of personal identification. The process of digitizing the signature is to measure the character image and to record the action of signature. For example, every character and the distinct speed, order, strength of each character are represented as

the individual's biometric features. This widespread method holds the advantage of easy public acceptance and fast implementation for personal security. The disadvantage is that each person will change the form of his/her signature with the changes of personality, the growth of experience and the changes of lifestyle. Voiceprint recognition technology (Jian et al. 2013; Hsieh et al. 2012; Chen et al. 2012) is performed through the analysis of one or more voice signals to achieve the identification of unknown sounds (Hsieh et al. 2012). The voiceprint signal process includes pre-emphasis, frame capture, window setup and spectrum analysis. The identity identification and semantics can be determined by comparison with a database (Chen et al. 2012; Assefi et al. 2015). However, the results of measurement and comparison will be directly affected by the changes in the quality and volume of the audio source. More pressingly, the identification system may be more easily deceived by pre-recorded sound.

Because the exterior biological features of human beings may be easily damaged and counterfeited, interior features have the advantage of uniqueness and authenticity. In fact, the finger-vein will show clearly visible characteristics when exposed on near infrared rays whose wavelengths are located between 700 and 1000 nm (Zhi and Shangling 2012). Recently the scholars and researchers have focused on finger-vein recognition due to its high security and living recognition (Zhi and Shangling 2012; Kumar and Zhou 2012; Qin and El-Yacoubi 2017). Afterwards, some well-known analysis such as principal components analysis (PCA) (Teoh and Rosdi 2011), Radon transform method (RTM) (Desong et al. 2010), local binary pattern (LBP) (Kuan et al. 2012), K-support Vector Machine Classifier (Veluchamy and Karlmarx 2017; Khellat-kihel et al. 2014) have gradually been applied to identify the finger-vein images. These investigations normalize vein images and compute the data of each image with tailored algorithms. However, some of the finger-vein images lack the clear texture of blood vessels due to physical structure of the individual's fingers. A lower rate of finger-vein recognition may occur if those unclear segmentations are processed and converted together with the other clear segmentations.

Therefore, it is an important topic to enhance the rate and stability of finger-vein recognition by distinguishing unclear textures of blood vessels using characteristics of the finger-vein images. In this paper, we propose a 'Four-Segmentations' methodology. First, the images shall be divided on basis of special local characteristics. Then, eigenvalues of the segmentation will be found by quantifying each segmental values through a statistical histogram and saved into the database for reference and comparison. Finally, the rate of finger-vein recognition will be enhanced by adjusting the weighted criteria of the four segmentations based on physiological structural conditions.

2 Proposed method

2.1 System architecture

In the study of finger-vein recognition the images will be affected by the tester's finger size and finger position inside device. And so, size and position are key topics to improving the sampling accuracy and identification performance of finger-vein images.

When the device recognized participants' fingers, the surface between fingers and the contact surface may not be horizontal. That is, images from the same subject may vary. To solve this problem, as Fig. 1 indicates, this article uses a servomotor to make the roller take pictures for finger-veins by slight rotations. This allows the system to calculate the dimension of vertical view. From these observations, the largest dimension is the best recognizing image of the horizontal surface between fingers and the contact surface.

The process of the vein-recognition system using standardized finger-vein images includes image preprocessing for capturing the vein image, image segmenting for confirming the boundary of segmentation, model training for computing the similarity with histogram of each segmentation, and model matching for obtaining the entire similar image by correction with respect to weighted criteria. The structure of the proposed finger-vein recognition system as Fig. 2 details is divided into two modes. The training mode regulates the database of testers' features. The testing mode preprocesses the tester's finger-vein images, captures their features, and then compare those features with ones in the database one-by-one and reports the final results.

The main units of the proposed finger-vein recognition system include image preprocessing, model training, model matching in original finger-vein images, and weight setup in finger-vein segmentation, detailed in the following sections.

2.2 Image preprocessing

The procedure of image preprocessing as Fig. 3 includes gray scale, median filter, edge detection, morphology, angularity correction, ROI (region of interest) Search, and Normal Form. 'Gray Scale' refers to the gray scale conversion of finger-vein image. The pixels of each specific point in the image will be converted to 0–255, and then the salt and pepper noise of the image will be eliminated by a median filter. Like the 3×3 mask, for example, the average of each pixel will be calculated and then the aberrant values will be replaced by the average value. Note that the mask size and error (ε) is related to the image.

Edge detection is used to detect the boundary of the finger in the finger-vein image. The image has strong changes of light source due to the cut-off of the finger's edge (Kang and Park 2010), so we utilized Sobel edge detection to deal with this problem (Kanopoulos et al. 1988). According to Eqs. (1), (2) the horizontal and vertical pixels will be computed separately and then the gradient size will be calculated with respect to Eq. (3). The objective is to find the edge of the finger in the image in order to separate the finger and background as Fig. 4.

$$G_x = \begin{bmatrix} -1 & 0 & +1 \\ -2 & 0 & +2 \\ -1 & 0 & +1 \end{bmatrix} \times A \tag{1}$$

$$G_y = \begin{bmatrix} -1 & -2 & -1 \\ 0 & 0 & 0 \\ +1 & +2 & +1 \end{bmatrix} \times A \tag{2}$$

$$G = \sqrt{G_x^2 + G_y^2} \tag{3}$$

After edge detection of the image, there will often be disconnections or lesser amounts of noise. Through the morphological method, small noise can be filtered by erosion as shown in Fig. 5a. Afterwards, the edge in the
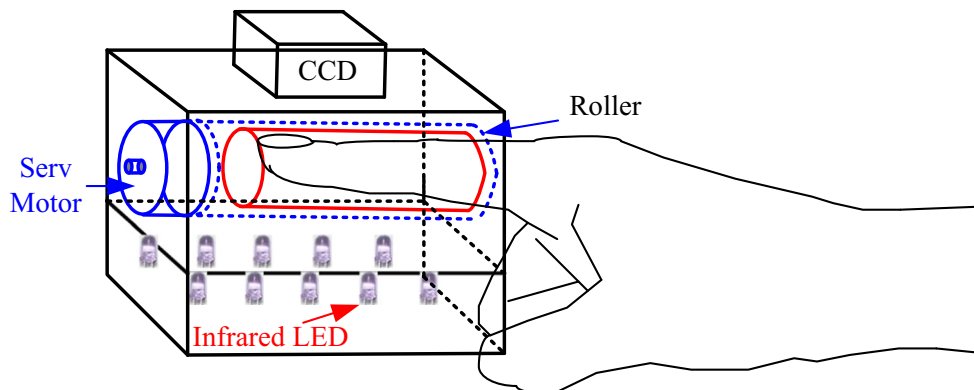
Fig. 1 Servomotor micro-control capture images
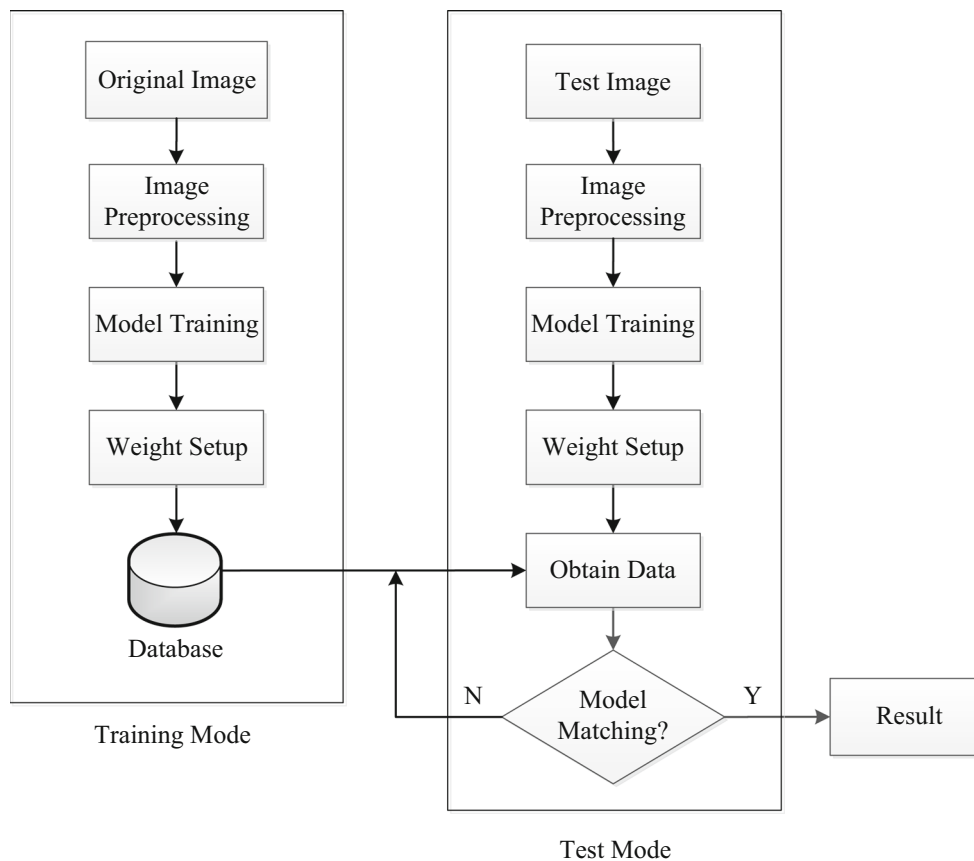
Fig. 2 System framework
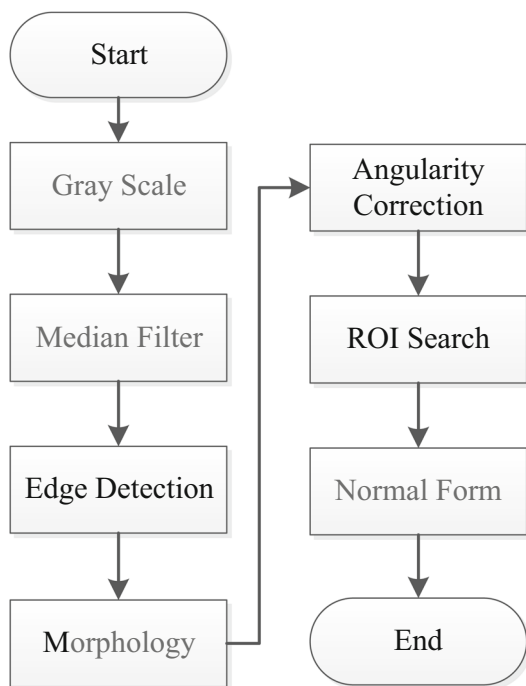
Fig. 3 Flowchart of image preprocessing

image will be compensated back to normal size by the expansion approach. Meanwhile, the broken section will be repaired as shown in Fig. 5b. The excess section of compensated image will be filtered by the erosion approach as shown in Fig. 5c. Finally, the result of morphological method is represented as shown in Fig. 5d.

As the fingers are placed into the instrument for measurement, the fingers may not be placed in the proper position for photography. The edge angle of fingers shall be corrected horizontally to capture their features. The horizontal correction rotates the image based on the angle between diagonal line of the finger and the middle line of the image. To achieve the rotational angle, the horizontal centerline colored in red in the image as Fig. 6a shall be confirmed firstly, and then the average centerline of upper and lower edges of the finger colored in orange in the image as Fig. 6a will be computed. The interpolated angle between the two straight lines is the angle for horizontal correction. The image with horizontal correction is shown as Fig. 6b.

Now the boundary of ROI shall be confirmed. The search target is the rectangular image of the largest area

Fig. 4 Result of edge detection. **a** Finger-vein image. **b**) Edge detection
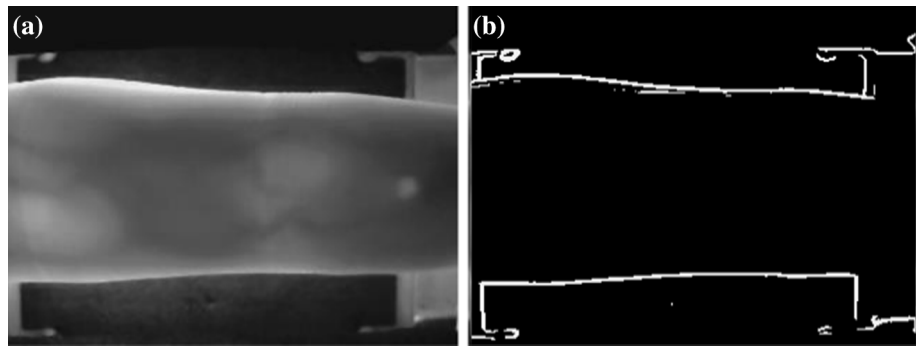
Fig. 5 Procedure of morphological method. **a** Filtered erosion. **b** Expansion approach repair broken section. **c** Back to normal size. **d** Result of morphological method
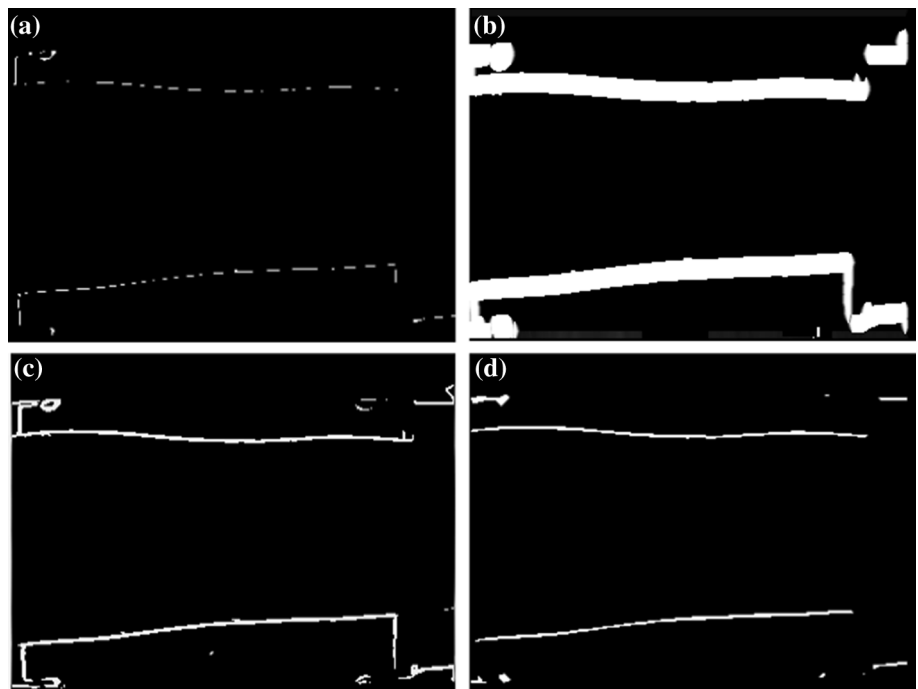
Fig. 6 Calculation result of diagonal line correction. **a** Diagonal line calculation. **b** Result of rotation correction
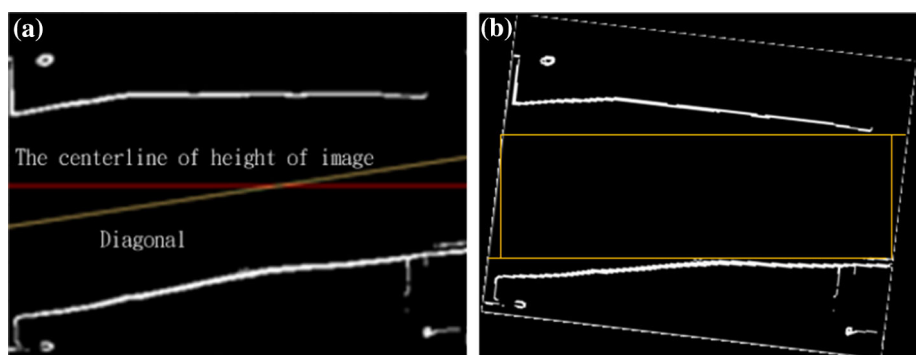
inside the edge of the finger. First, the largest y-axis coordinate of pixels belongs to the edge of the finger above the centerline in the image, as Fig. 7a illustrates, is found by scanning the image from the centerline to the top. Afterwards, the smallest y-axis coordinate of pixels as seen in Fig. 7b is found by scanning the image from the centerline to the bottom. The upper and lower boundaries of rectangular area in the ROI, Fig. 7c, are obtained by extending the two coordinates horizontally. Finally, the pixels of the original image will be recovered on the basis of the ROI as Fig. 7d.
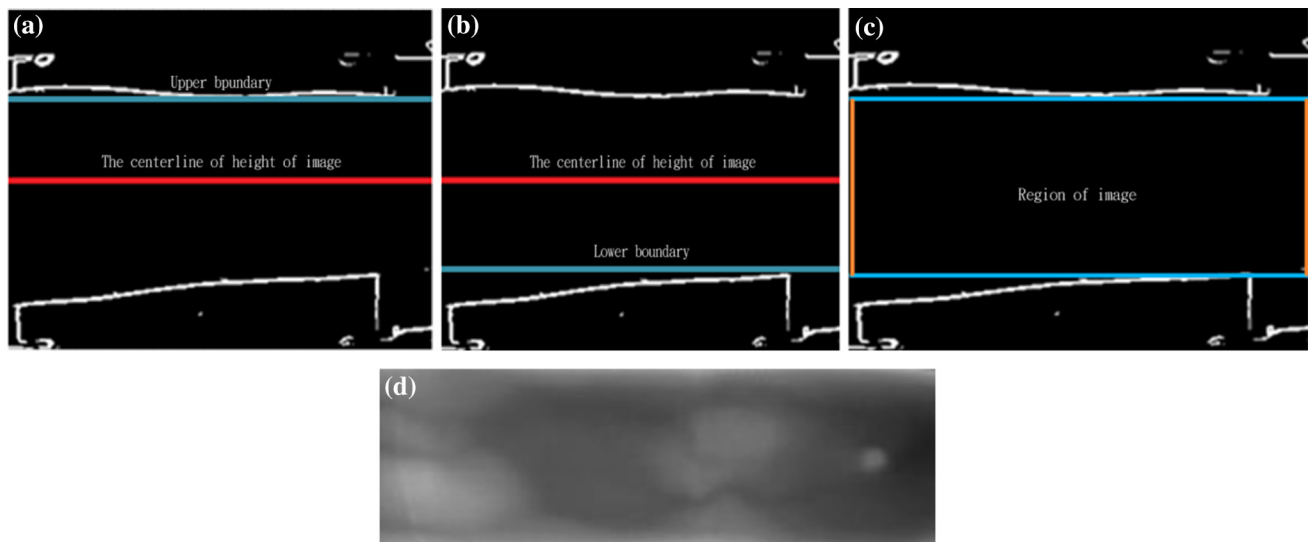
Fig. 7 Procedure of ROI boundary search. **a** On top of edge search. **b** On botton of edge search. **c** ROI boundary section. **d** Recovered on the basis of the ROI

Since the size of ROI captured by the finger-vein image is variable for each person, the image will be normalized by the 'Nearest Neighbor' method (Batchelor 1977). The finger-vein image, with an aspect ratio of 3:1, will be converted into 180×60 through the normalization process.

2.3 Model training

As the finger-vein image is captured via irradiation of near-infrared light between 700 and 1100 nm, the image will have strong and significant changes within light and shade in Fig. 8. The changes are caused by the degree of light transmission between the bone of muscles and joints. Therefore, this special condition can be applied to determine the segmentation of the finger-vein image. When the adaptive segmentation of the vein image is performed, the image is first processed smoothly by a mask. In this paper, the 5×5 mask will slide on the original image, and the average value of the overlapping pixels between the image and the mask is calculated as the regional threshold value T as shown in Fig. 9. The value of T is calculated as Eq. 4.
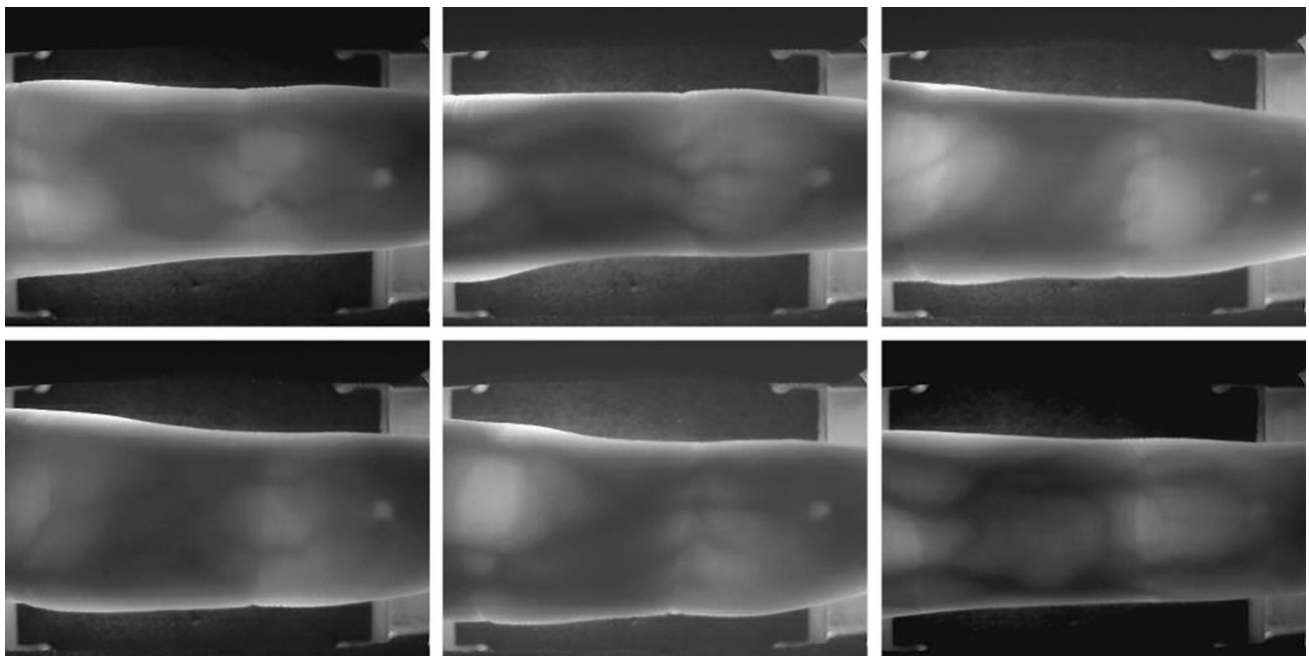
Fig. 8 Finger-vein image of different tester
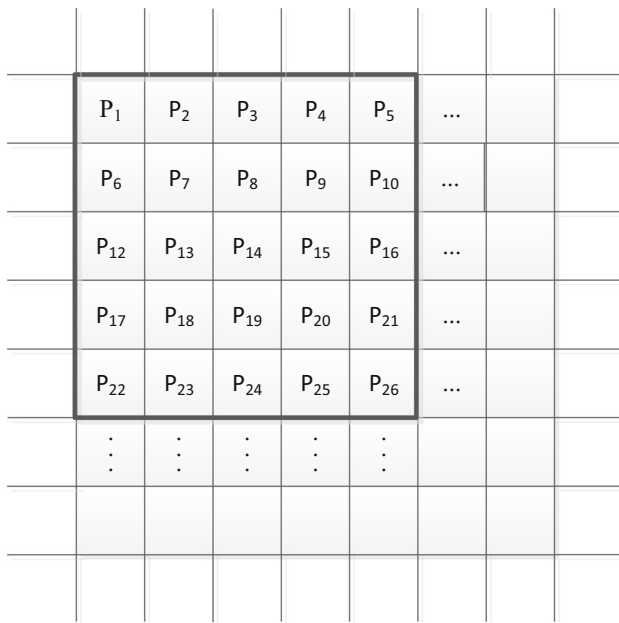
Fig. 9 Mask value

These steps will be repeated until the area of the threshold image is established to complete the mask. The overall flow chart of calculation for the threshold image is shown as Fig. 10.

$$T = \frac{\sum_{i=1}^{n} Pi}{n} \tag{4}$$

After calculating the image threshold value T, the T value is overlapped with the same coordinate position pixel of the original image, and then the threshold value is compared with the image F to obtain the local threshold value by using the formula displayed by Eq. 5. The threshold value by this method can be adapted to the intensity of light changes. For example, the average threshold value increases with respect to the strong light, and conversely, the average light threshold decreases. After filtering the image via the threshold value, we compute the white pixels of vertical direction by using statistics to confirm the boundary between light and shade according to the quantity of local threshold points in the image. Finally, the dynamic boundary can be determined by the size of the statistics. The final segmentation result is shown as Fig. 11.

$$\begin{cases} f(x,y) = 0 & f(x,y) \geq T(x,y) \\ f(x,y) = 255 & f(x,y) < T(x,y) \end{cases} \tag{5}$$

2.4 Model matching

The model matching includes histogram statistics and histogram comparison. The details are described as follows:
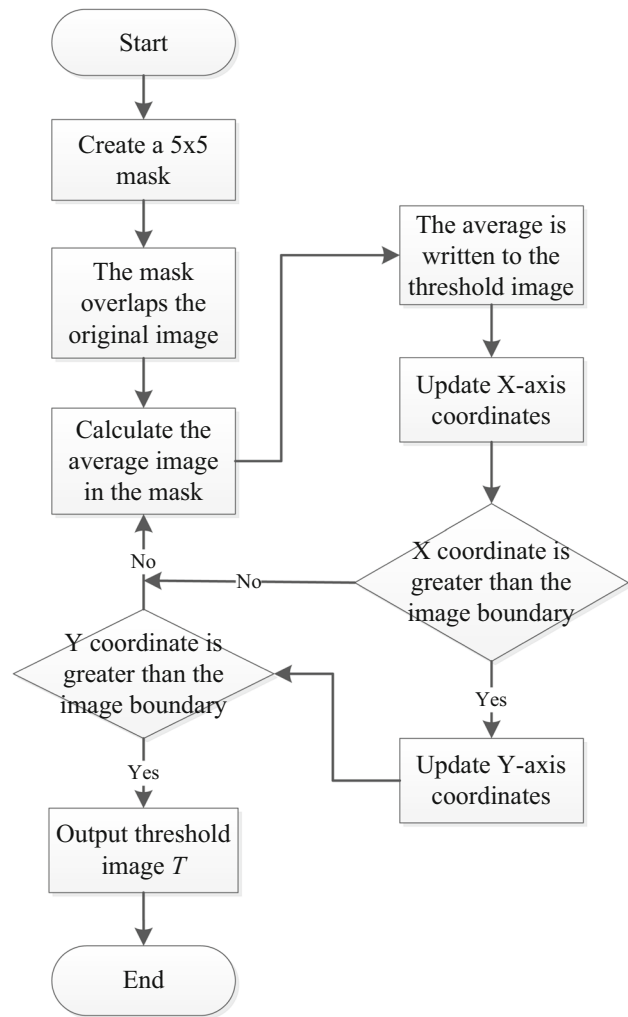
Fig. 10 Flow chart of threshold image calculation

1. Histogram statistics: The vein image through the adaptive segmentation will be divided into four segmentations as shown in Fig. 12. The changes of finger-vein image by irradiation of near-infrared rays will represent the physiological features of the segmentations. The result of histogram statistics after quantification is as shown in Fig. 13.

2. Histogram matching: The histogram matching belongs to a sample of statistics. Bhattacharyya distance conversion combined with the weighted method of statistics can be applied to compare the similarity of two statistical samples. The Bhattacharyya distance is an algorithm to measure the distribution of two discrete probability (Sungwook and Chulhee 2013). Its definition is described in Eq. 6, where p and q represent two different discrete probability distributions, and Bhattacharyya Coefficient (BC) is shown in Eq. 7
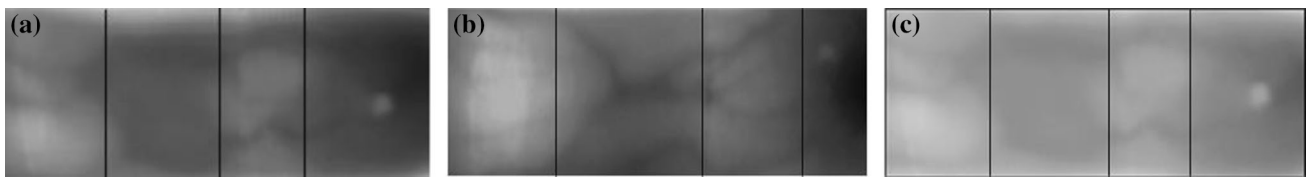
Fig. 11 Adaptive segmentation result of three finger-vein image
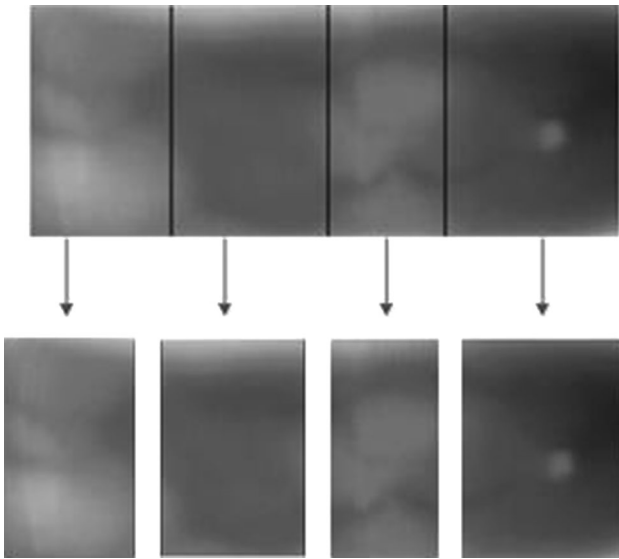
Fig. 12 Segmentations of finger-vein image

$$\mathrm{DB}(p,q) = -\ln(BC(p,q)),\ 0 \leq \mathrm{DB} \leq \infty \qquad (6)$$

$$\mathrm{BC}(p,q) = \sum_{i=0}^{255} \sqrt{p(x) \times q(x)},\ 0 \leq \mathrm{BC} \leq 1 \qquad (7)$$

The closer to zero the value calculated by the Bhattacharyya distance is, the greater the similarity shared by the two compared histograms is. The different finger-vein image of the index finger belongs to one tester via Bhattacharyya distance conversion is shown as Fig. 14a, and the finger-vein image of the index finger belonging to another tester is shown as Fig. 14b.

We observe that the value of Bhattacharyya distance conversion of different finger-vein images belonging to one person will be relatively low. Meanwhile, the value of Bhattacharyya distance conversion in the darker images will be high. During finger-vein test, we will have two different four-segmentation images processed by model matching and histogram calculation, and then compare the Bhattacharyya distance of those four-segmentation images with the original image of the database. Afterwards, the weight of the image corresponding to the degree of transmission will be adjusted so that the influence of the computed result caused by less information of segmentations will be reduced.
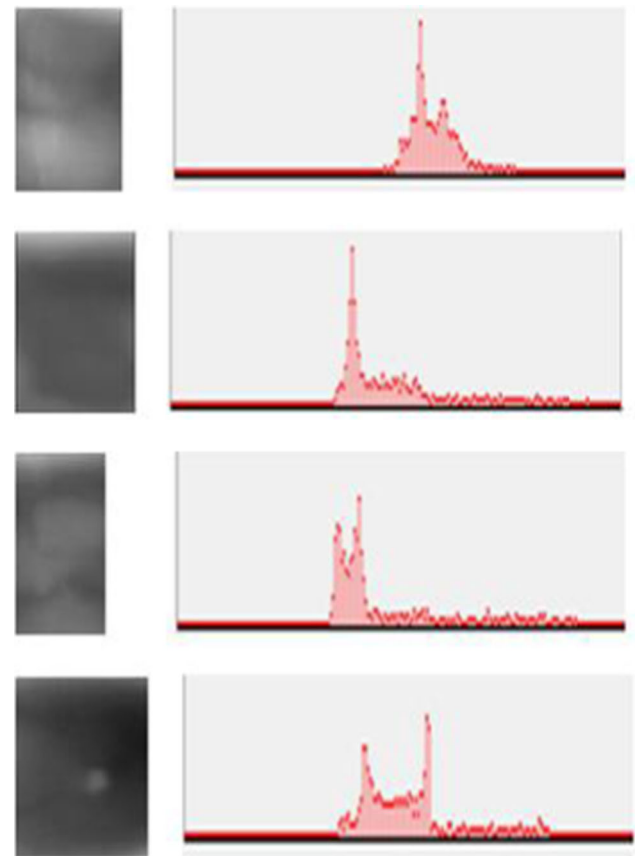
Fig. 13 Histogram statistics result of finger-vein image

2.5 Weight setup

The higher value of the Bhattacharyya distance between the second and fourth darker images can be observed in Fig. 13. The values of the second and fourth segmentations will be 0.334 and 0.22. Due to the low recognition of the two segmentations, their weights shall be reduced. The corresponding weights of each segmentation will be α_1, α_2, α_3, α_4 as Tables 1 and 2.

Here:

$$w_1 + w_2 + w_3 + w_4 = 1 \qquad (8)$$

The overall histogram difference, w_t, can be calculated with respect to the weights in Table 3:

$$w_t = \alpha_1 w_1 + \alpha_2 w_2 + \alpha_3 w_3 + \alpha_4 w_4 \qquad (9)$$

(a)

(b)
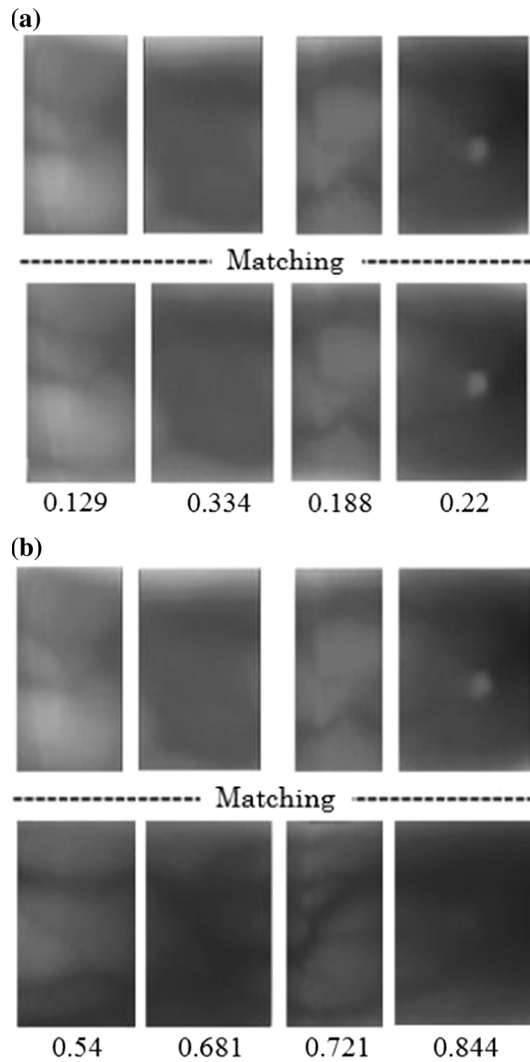
Fig. 14 The result of Bhattacharyya distance. **a** Conversion result of the same finger-vein image. **b** Conversion result of different finger-vein image

Table 1 Corresponding weights

α_1	α_2	α_3	α_4
w_1	w_2	w_3	w_4

Finally, the value of w_t shall be compared with the predetermined threshold value of T. If the value of w_t is greater than T, the finger-vein image will be regarded as belonging to the same person. Otherwise, the image will be determined to be another person's finger-vein image. The judgment rule is given as Eq. 10.

$$\begin{cases} w_t \geq T & True \\ w_t < T & False \end{cases} \tag{10}$$

In this way, the vein image can be processed step-by-step through the described methods so as to finally find the value of the features for comparison. Therefore, this data

Table 2 Experiment compare of different fingers catching image

Tester	Finger placement type	Width (mm)	Area(mm^2)
A	Type A1	13.737	724.446
	Type A2	15.894	789.438
	Type A3	16.800	821.235
	Type A4	14.261	754.295
	Type A5	14.824	669.732
B	Type B1	15.260	742.818
	Type B2	16.034	762.507
	Type B3	17.147	839.946
	Type B4	16.186	707.947
	Type B5	15.789	694.806

Table 3 Parameters of the experiment

Item	Parameter
Training images/person	1
Matching images/person	6
Random matching times	100
Quantity of persons	106

can be used to confirm the identity of the user who provided the vein image to the system to achieve the objective of identity recognition.

3 Experimental results and discussion

The system of this study was developed on a PC platform installed with 64-bit Windows7 Enterprise Edition System Service Pack 1 designed by Microsoft Corporation. CPU is Intel (R) Core (TM) i7-2600 CPU@3.40 GHz with a memory of 6 GB RAM. The programming language of finger-vein image recognition is written by using the C # high-level object-oriented programming language developed by Microsoft, and the development environment enlisted was Visual Studio integration development environment for C # program development. The image database used in this study is the finger-vein database of the Group of Machine Learning and Applications, Shandong University (SDUMLA) (SDUMLA-HMT Database 2017). The finger-vein images are from an Asian-based database. In this study, the finger-vein images belong to 106 persons included in the database. The samples included individuals from industry, business, and academia who were between 20 and 60 years old. The complexity of the user's entire database is representative, and the index finger, middle
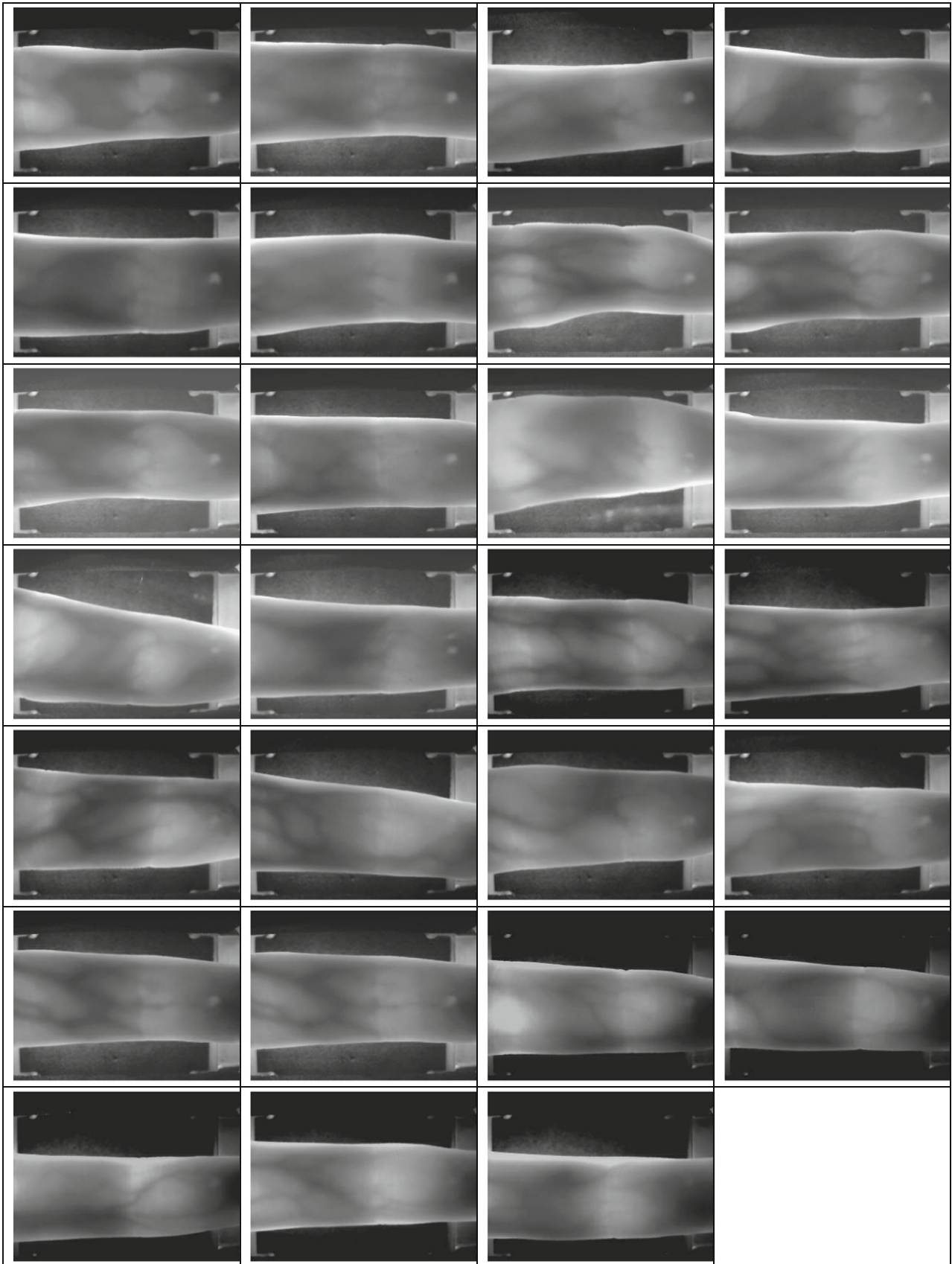
Fig. 15 Finger-vein images database

finger, and little finger of both hands were sampled. Each subject's finger was sampled by six images. The quantity of finger-vein images was 3816. The sample of finger-vein images included in the database is shown as Fig. 15.

3.1 The standardizing processing experiment of finger-vein image

As Fig. 1, we conduct measuring experiment of five different fingers for largest dimension and width by two researchers' fingers. The result is Fig. 16 and the illustration is Fig. 2. We can know the Type A3 and Type B3 have the largest width and dimension.

3.2 Finger-vein recognition experiment

To verify that the method proposed in this paper has improved the accuracy of finger-vein recognition, we have carried out global vein image recognition, fixed segmentation vein image identification, dynamic segmentation vein image recognition and compared the different weighted values of adaptive segmentation finger-vein recognition which includes physical physiological conditions.

In the experiment, each data of finger-vein image shall be normalized by the 'Nearest Neighbor' method. Each finger has six different vein images. The finger-vein image
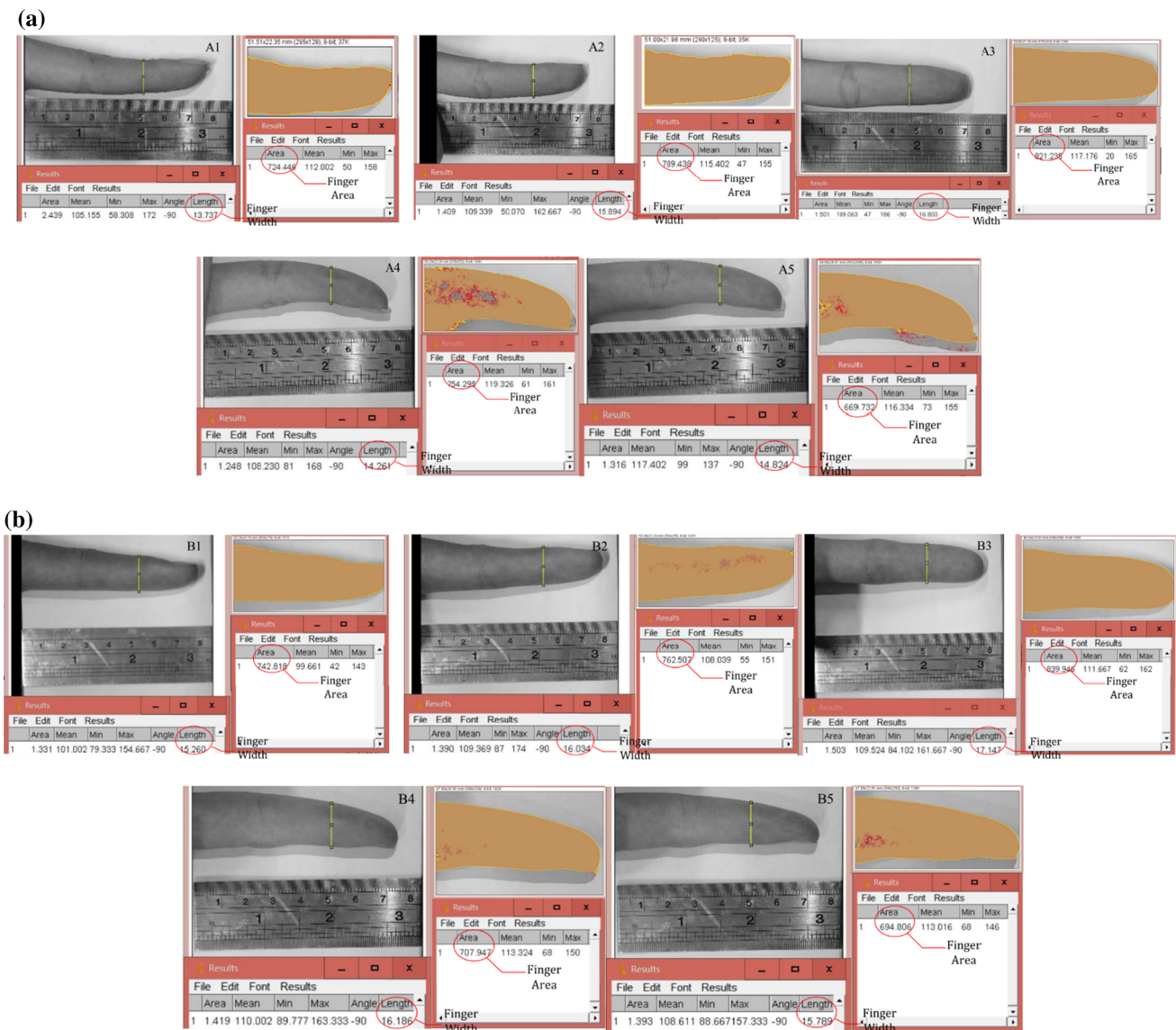
Fig. 16 Measuring experiment of different fingers catching image. **a** Tester A. **b** Tester B

Fig. 17 The comparison of global vein recognition

(a)

(b)
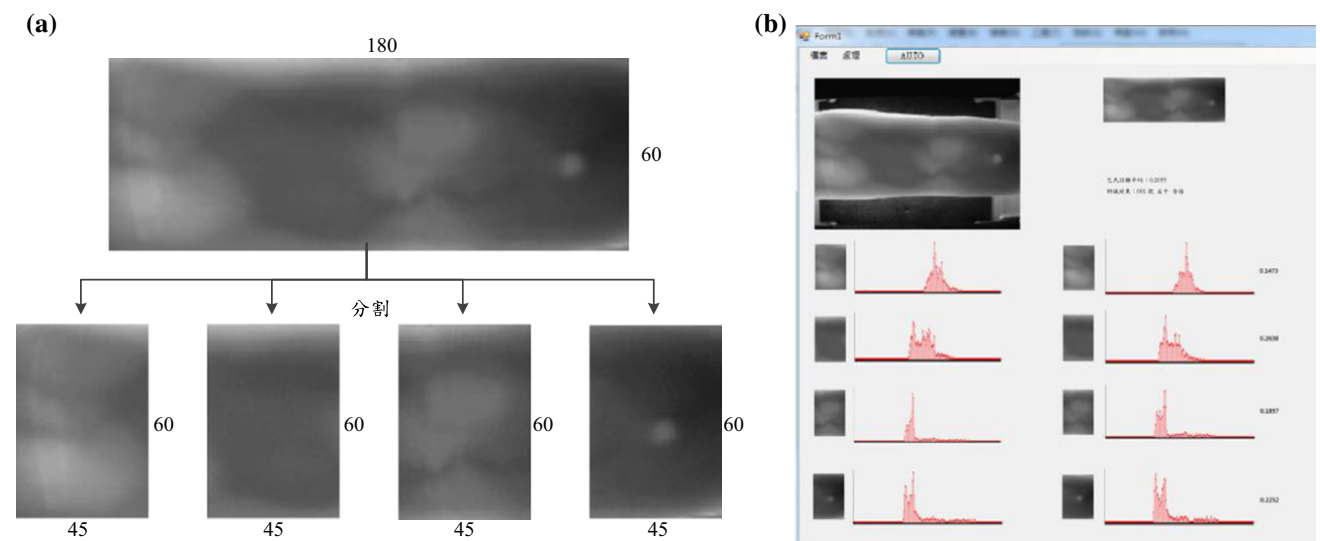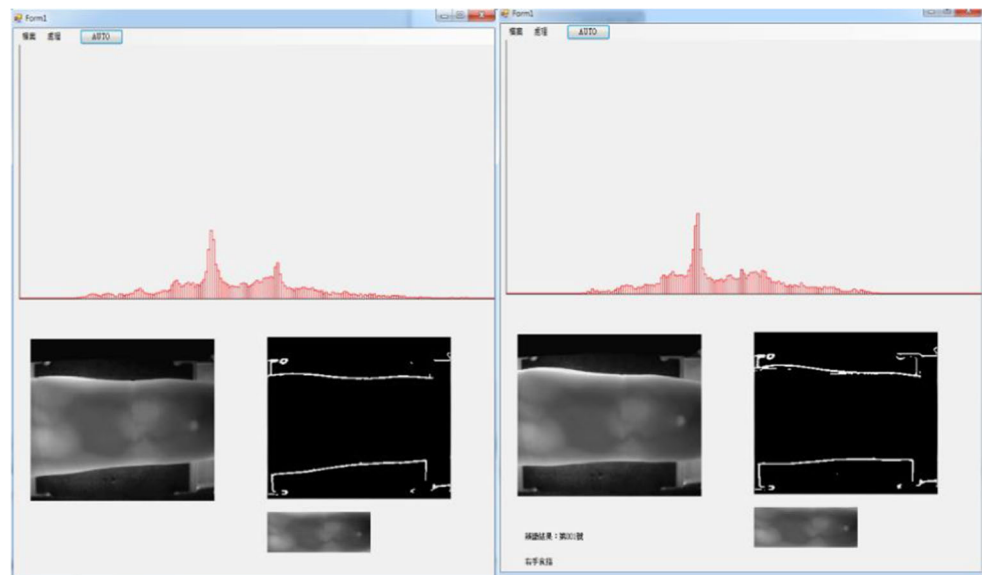
Fig. 18 Fixed segmentation finger-vein recognition. **a** Fixed segmentation vein image. **b** Comparison of fixed segmentation

saved in the database for recognition is chosen randomly within the six different vein images. Afterwards, one of 6 vein images will be randomly selected to compare with the data in the database up to 300 times. The parameters of the experiment are shown in Table 3.

The three finger-vein image recognition methods discussed and compared included global vein identification, fixed segmentation finger-vein image recognition, and adaptive segmentation finger-vein image recognition. The global vein identification utilizes the histogram statistics based on the entire ROI area to achieve the objective of identification. The fixed segmentation finger-vein image recognition method normalizes the ROI into the size of 180:60, and then divide it into 4 segmentations independently as in Fig. 16. Afterwards, the histogram statistics

and similarities of each segmentation will be compared. Finally, for the adaptive segmentation finger-vein image recognition method proposed by this study, the ROI found in the experiment was 180:60 after normalization, and the image was divided into four segmentations by the dynamic boundary. Afterwards, the result of recognition will be obtained through histogram statistics and similarity comparison. The experiments of three recognition methods were sampled 20, 40, 60, 80, and 100 with respect to 106 testers. The recognition image of the three methods is shown in Figs. 17, 18 and 19. We have learned from Table 4 that the average rate of global vein identification is about 74.55% and the average recognition rate of the finger-vein image is about 86.48%. The average recognition rate of the adaptive segmentation finger-vein image is

(a)

(b)
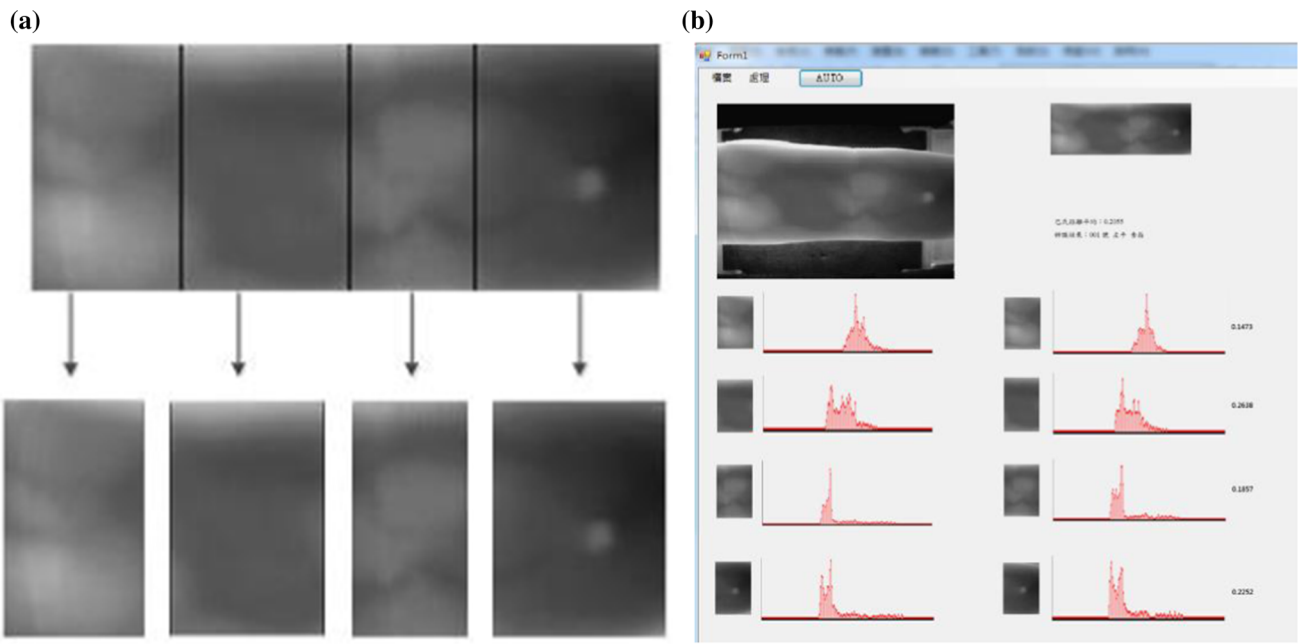
Fig. 19 The experiment of adaptive finger-vein segmentation recognition. **a** Adaptive finger-vein segmentation. **b** Comparison of adaptive segmentation

Table 4 Comparison of recognition rate

Sample	Successful recognition/recognition rate		
	Global vein recognition	Fixed segmentation vein recognition	Adaptive segmentation finger-vein recognition
20	15/75.00%	17/85.00%	18/90.00%
40	28/70.00%	35/87.5%	37/92.50%
60	48/80.00%	52/86.67%	56/93.33%
80	59/73.75%	69/86.25%	74/92.50%
100	74/74.00%	87/87.00%	92/92.00%

Table 5 Experiment of corresponding weights

w_1 (%)	w_2 (%)	w_3 (%)	w_4 (%)	Recognition rate (%)
25	25	25	25	92.06
25	25	30	20	94.37
25	25	35	15	94.84
30	20	35	15	97.00
30	20	30	20	95.67
35	15	35	15	96.33

about 92.06%, and it is significantly higher than the other two methods.

Next, the physiological structural conditions are added into the recognition rate with the weight coefficients, and the experimental results are shown in Table 5. We have learned from Table 5 that the highest recognition rate is 97% under the conditions of $w_1 = 30\%$, $w_2 = 20\%$, $w_3 = 35\%$, $w_4 = 15\%$. These results show that the adaptive segmentation finger-vein image recognition, which includes physiological structural conditions, significantly improves finger-vein image recognition.

4 Conclusions

Technological advances create novel conveniences, but in their process of invention, they also create novel security problems. Finger-vein recognition, enlisting the uniqueness of living recognition, is a high security biometric identification technology that has gradually been commercialized and applied to ATM and other industries calling for a high degree of security in identity verification. In this paper, a regional segmentation method is proposed to divide the finger-vein image according to the physiological features of the finger, and then the recognition rate of the finger-vein image will be enhanced by adding local weights

according to local vertical statistics of each segmentation. The experimental results show that among the 106 adults aged 20–60 years old the rate of adaptive segmentation finger-vein recognition will reach 97% in 3816 finger images, comparatively superior in accuracy to global vein recognition at 74.55%, and fixed segmentation vein recognition at 86.48%. The research methodology will provide other well-known research methods such as principal components analysis (PCA), Radon transform method (RTM), and local binary pattern (LBP) to further enhance the fidelity of finger-vein recognition.

References

Anjomshoa F, Aloqaily M, Kantarci B, Erol-Kantarci M, Schuckers S (2017) Social behaviometrics for personalized devices in the internet of things era. IEEE Access 5:12199–12213

Assefi M, Wittie M, Knight A (2015) Impact of network performance on cloud speech recognition. In: 2015 24th International conference on computer communication and networks, pp 1–6

Batchelor BG (1977) Faster nearest-neighbour calculations. Electron Lett 13(10):304–306

Chang YL, Han HC, Fan KC, Chen KS, Chen CT, Chang JH (2003) Greedy modular eigenspaces and positive Boolean function for supervised hyperspectral image classification. Opt Eng 42(9):2576–2587

Chen WP, Chen SS, Lin CC, Chen YZ, Lin WC (2012) Automatic recognition of frog call using multi-stage average spectrum. Comput Math Appl 64(05):1270–1281

Chiranjeevi P, Gopalakrishnan V, Moogi P (2015) Neutral face classification using personalized appearance models for fast and robust emotion detection. IEEE Trans Image Process 24(9):2701–2711

Desong W, Jianping L, Memik G (2010) User identification based on finger-vein patterns for consumer electronics devices. In: IEEE transactions on consumer electronics, vol 56, no 2, pp 799–804, May 2010

Hong Lin, Jain Anil (1998) Integrating faces and fingerprints for personal identification. IEEE Trans Pattern Anal Mach Intell 20(12):1295–1307

Hsieh SC, Chen WP, Lin WC, Chou FS, Lai JR (2012) A study on the application of an average energy entropy method for the endpoint extraction of frog croak syllables. Taiwan J For Sci 27(2):149–161

Jabbar H, Jeong T, Hwang J, Park G (2008) Viewer identification and authentication in IPTV using RFID technique. IEEE Trans Consum Electron 54(1):105–109

Jain AK, Arora SS, Cao Kai, Best-Rowden L, Bhatnagar A (2017) Fingerprint recognition of young children. IEEE Trans Inf Forensics Secur 12(7):1501–1514

Jayasekara B, Jayasiri A, Udawatta L (2006) An evolving signature recognition system. In: First international conference on industrial and information systems, pp 529–534, August 2006

Jian H, Jianbin Z, Huaqiao X, Enqi Z (2013) Voiceprint identification based on model clustering. In: International conference on communications and networks, pp 727–730, November 2013

Kai C, Jain AK (2015) Learning fingerprint reconstruction: from minutiae to image. IEEE Trans Inf Forensics Secur 10(1):104–117

Kang BJ, Park KR (2010) Multimodal biometric method based on vein and geometry of a single finger. Inst Eng Technol 4(3):209–217

Kanopoulos N, Vasanthavada N, Baker RL (1988) Design of an image edge detection filter using the Sobel operator. IEEE J Solid State Circuits 23(2):358–367

Khellat-Kihel S, Abrishambaf R, Cardoso N, Monteiro J, Benyettou M (2014) Finger vein recognition using Gabor filter and support vector machine. In: International image processing, applications and systems conference, pp 1–6, 2014

Kuan WQ, Khisa AS, Xiang WQ, Qiu ZS (2012) Finger vein recognition using LBP variance with global matching. In: 2012 international conference on wavelet analysis and pattern recognition, pp 196–201, July 2012

Kumar A, Zhou Y (2012) Human identification using finger images. IEEE Trans Image Process 21(4):2228–2244

Li Z, Gong D, Li X, Tao D (2015) Learning compact feature descriptor and adaptive matching framework for face recognition. IEEE Trans Image Process 24(9):2736–2745

Li Y, Wang H, Sun K (2017) Personal information in passwords and its security implications. IEEE Trans Inf Forensics Secur 12(10):2320–2333

Ohtake G, Ogawa K, Safavi-Naini R (2015) Privacy preserving system for integrated broadcast-broadband services using attribute-based encryption. IEEE Trans Consum Electron 61(3):328–335

Qin H, El-Yacoubi MA (2017) Deep representation-based feature extraction and recovering for finger-vein verification. IEEE Trans Inf Forensics Secur 12(8):1816–1829

Ratha NK, Connell JH, Pankanti S (2015) Big Data approach to biometric-based identity analytics. IBM J Res Dev 59(2):4:1–4:11

SDUMLA-HMT Database (2017) Machine Learning and Applications, Shandong University (SDUMLA). http://mla.sdu.edu.cn/sdumla-hmt.html

Sungwook Y, Chulhee L (2013) Edge detection for hyperspectral images using the Bhattacharyya distance. In: International conference on parallel and distributed systems, pp 716–719, August 2013

Teoh BS, Rosdi BA (2011) Finger-vein identification using pattern map and principal component analysis. In: IEEE international conference on signal and image processing applications, pp 530–534, November 2011

Veluchamy S, Karlmarx LR (2017) System for multimodal biometric recognition based on finger knuckle and finger vein using feature-level fusion and k-support vector machine classifier. IET Biom 6(3):232–242

Xing X, Wang K, Lv Z (2015) Fusion of gait and facial features using coupled projections for people identification at a distance. IEEE Signal Process Lett 22(12):2349–2353

Zhi L, Shangling S (2012) An embedded real-time finger-vein recognition system for mobile devices. IEEE Trans Consum Electron 58(2):522–527